ORIGINAL PAPER

Evaluation of the effect of additive group five elements on the properties of Pb-Ca-Sn-Al alloy as the positive grid for lead-acid batteries

Baofeng Yang[1,2] · Xianyu Cai[2] · Enyu Li[2] · Shaoqiang Yang[1] · Wei Liu[1,2] · Changsong Dai[1,2] · Geping Yin[1]

Abstract

As an important part of lead-acid batteries, the grid is mainly used to support active substances and conduct current. Currently, Pb-Ca-Sn-Al alloys are widely used as materials for valve-regulated lead-acid battery grids. The influence of bismuth, barium, strontium, and germanium as alloying additives on the physical and electrochemical behaviors of Pb-Ca-Sn-Al alloys was studied by the methods of metallographic, cyclic voltammetry, linear scanning voltammetry, AC impedance, and scanning electron microscopy. The results show that the addition of Bi and Ba can increase the grain size of the alloy and reduce the intergranular corrosion and corrosion rate of Pb-Ca-Sn-Al alloy. Furthermore, the addition of Bi and Ba could inhibit the growth of Pb (II) and PbO_2 in corrosion layer and improve the corrosion resistance of the alloy. Significantly, Bi and Ba will reduce the oxygen evolution overpotential of the alloy by about 30 mV, which will play important roles on the maintenance-free performance of lead-acid batteries. Both Sr and Ge promote the grain corrosion and intergranular corrosion of the alloy, reducing the corrosion resistance of the alloy. Therefore, improving the performance and corrosion life of the grid by using additives is an important approach to further extending the service life of lead-acid batteries.

Keywords Pb-Ca-Sn-Al alloy · Grain · Corrosion rate · Corrosion layer · Corrosion resistance · Micro topography

Introduction

In recent years, lead-acid battery performance has been greatly improved with the development of the lead carbon technology, especially the service life [1–3]. As well demonstrated, the performance of the grid alloy, mainly the lead-antimony alloy and lead-calcium alloy [4, 5], plays an important role in the service life of lead-acid batteries. Lead-antimony alloys have occupied an important position for more than 100 years, which, however, cause water loss and affect battery life [6].

Due to the advantages of high hydrogen evolution overpotential and low water loss of lead-calcium alloy, it has been generally used in the maintenance-free lead-acid batteries. However, due to the high corrosion rate of lead-calcium alloy and the poor performance of deep cycling, its application is greatly inhibited [7, 8].

Recently, some studies have shown that adding additives to the alloy can improve the properties of corrosion resistance. For example, it has been demonstrated that adding bismuth can enhance the corrosion resistance and improve the comprehensive properties of the alloy [9, 10]. A.J. Li et al. [11] systematically studied Pb-La alloy and found that additive La can effectively inhibit the oxygen evolution reaction and the growth of Pb (II) oxides during the electrochemical tests. The addition of barium to the alloy can improve the corrosion resistance and reduce the growth rate of the alloy [12]. In addition, the additive Ag in the alloy can improve the mechanical strength of the alloy and refine the grain [13]. Grain refinement is an important way to improve the strength of the alloy and performance in lead-acid batteries. The refinement mechanism is related to the solidification process that takes

✉ Geping Yin
  yingeping@hit.edu.cn

1   MIIT Key Laboratory of Critical Materials Technology for New Energy Conversion and Storage and Institute of Advanced Chemical Power Sources, School of Chemistry and Chemical Engineering, Harbin Institute of Technology, Harbin 150001, Heilongjiang, People's Republic of China

2   Key Laboratory of Electrochemical Energy Storage Technology of Jiangsu Province, Shuangdeng Group Co., Ltd., Taizhou 225500, Jiangsu, People's Republic of China

place during which the intermetallic compounds' precipitate at the grain surface and the grain boundary, decreasing the nucleation energy and thereby achieving the grain refinement. The addition of Sm was found to refine the grains, inhibit the growth of the passivation layer, and increase the lead-acid battery life [14].

At present, lead-calcium-tin-aluminum quaternary alloys are used as the main materials for the grid of maintenance-free lead-acid batteries. In this paper, the electrochemical properties of Pb-Ca-Sn-Al alloy with different additives (Bi, Ba, Sr, and Ge) were studied. The purpose of adding these additives is to reduce the grain size and intergranular corrosion, which is hypothesized to slow the corrosion rate of the alloy. In addition, the physical properties and electrochemical performance are the key factors to determine whether the alloys can be used in long-life batteries. The results in this report are thus helpful to screen a suitable grid material for lead-acid batteries with enhanced service life.

Experimental

Materials' preparation

Pb-Ca-Sn-Al alloy (weight ratio: Sn/Ca $\approx$ 30, the content of Ca is about 0.05 wt.%, and the content of Sn is about 1.5 wt.%) was used as a blank and reference sample in this study. The group V elements were introduced into the comparative sample to make a Pb-Ca-Sn-Al-X pentanary alloy. The addition ratio of the alloy additive is about 0.015 to 0.03%, considering the results of other researchers' studies and the cost of the alloy. The samples were prepared by melting weighed mixtures of pure lead (99.994%), calcium (99.9%), tin (99.99%), aluminum (99.7%), bismuth (99.99%), barium (99.9%), strontium (99.5%), and germanium (99.999%) in an electrical furnace. First, Pb is cast into master alloys with Bi, Ba, Sr, and Ge, respectively, and then placed in a graphite crucible with Pb, Sn, Al, and Pb-Ca master alloy, stirred, and melted uniformly in electric resistance furnace for 1 h at 600 °C under argon protection. Finally, the desired alloy is obtained. The compositions of the of Pb-Ca-Sn-Al (weight ratio: Sn/Ca $\approx$ 30)-1%X (X stands for Bi, Ba, Sr, and Ge) alloys were measured by optical emission spectrometer (ARL 4460, Thermo Scientific) and ICP (Plasma 2000, China Iron & Steel Research Institute Group). The proportion of different additives are listed in Table 1. It is considered acceptable that the composition of the test alloy may have a slight deviation due to the alloy burned during the configuration process. The electrode rods with a 1 cm^{-2} end surface and the other surfaces were sealed with epoxy resin to serve as the working electrodes. The end surface of the test sample as the working surface was polished on a Grinder-Polisher (EcoMet 250, BUEHLER) using 400#, 1000#, and 2500# sandpapers in

Table 1 The proportion of different additives in Pb-Ca-Sn-Al

Numbers	Additives	Amounts (wt.%)
1#	–	–
2#	Bi	0.030
3#	Ba	0.015
4#	Sr	0.027
5#	Ge	0.019

sequence [15], until there were no obvious scratches on the surface under the microscope.

Performance testing

The samples were immersed in a chemical polishing solution (75% acetic acid + 25% hydrogen peroxide) for several seconds after there were no obvious scratches on the surface, then observed under a metallographic microscope (MA100L, Nikon) after washing and drying. The polished alloy samples were measured for its hardness on a Vickers hardness tester.

Electrochemical tests were performed in a three-electrode configuration using electrochemical working station (PGSTAT 302N Autolab, EcoEchemie B.V. Company/CH Instrument Model 660, Shanghai Chen Hua Technology Co., Ltd). The counter and reference electrodes were a platinum plate (4 cm^2) and Hg/Hg$_2$SO$_4$/K$_2$SO$_4$ (MSE) electrode (having a potential of 0.645 V vs. NHE), respectively. All potentials reported in this paper were referred to this electrode. The electrolyte was 1.28 g cm^{-3} sulfuric acid solution, and all the tests and analysis were carried out at 25 °C.

The anodic oxygen evolution test was performed after the test electrodes have been maintained at 1.6 V for 1 h to form a stable oxide layer on the surface of the electrodes. The test was performed between 0.6 V and 1.8 V at a sweep rate of 5 mV s^{-1}.

All the alloy electrodes were polarized at − 1.2 V for 20 min to remove the corrosion layer on the surface before the cathodic hydrogen evolution test and cyclic voltammetry test. The electrodes for cathode hydrogen evolution test were scanned at − 1.0 to − 1.8 V at a sweep rate of 5 mV s^{-1}. The cyclic voltammetry tests were performed 50 cycles between 0.6 V and 1.6 V at a sweep rate of 5 mV s^{-1}.

The linear sweep voltammetry and electrochemical impedance spectroscopy were performed after the electrodes have been polarized for 1 h at 0.9 V. The linear sweep voltammetry was scanned from 0.9 to − 1.2 V with a scanning rate of 2 mV s^{-1}. In the electrochemical impedance spectroscopy, the amplitude was 5 mV, and the applied frequency was from 10^5 to 10^{-1} Hz.

Corrosion tests were carried out in a three-electrode system by cyclic voltammetry in the electrolyte of 1.28 g cm^{-3} H$_2$SO$_4$ at 50 °C. The working electrode was the measured alloy

Fig. 1 The metallographic structure of different Pb-Ca-Sn-Al alloys. (1#: Pb-Ca-Sn-Al; 2#: Pb-Ca-Sn-Al-Bi; 3#: Pb-Ca-Sn-Al-Ba; 4#: Pb-Ca-Sn-Al-Sr; 5#: Pb-Ca-Sn-Al-Ge)
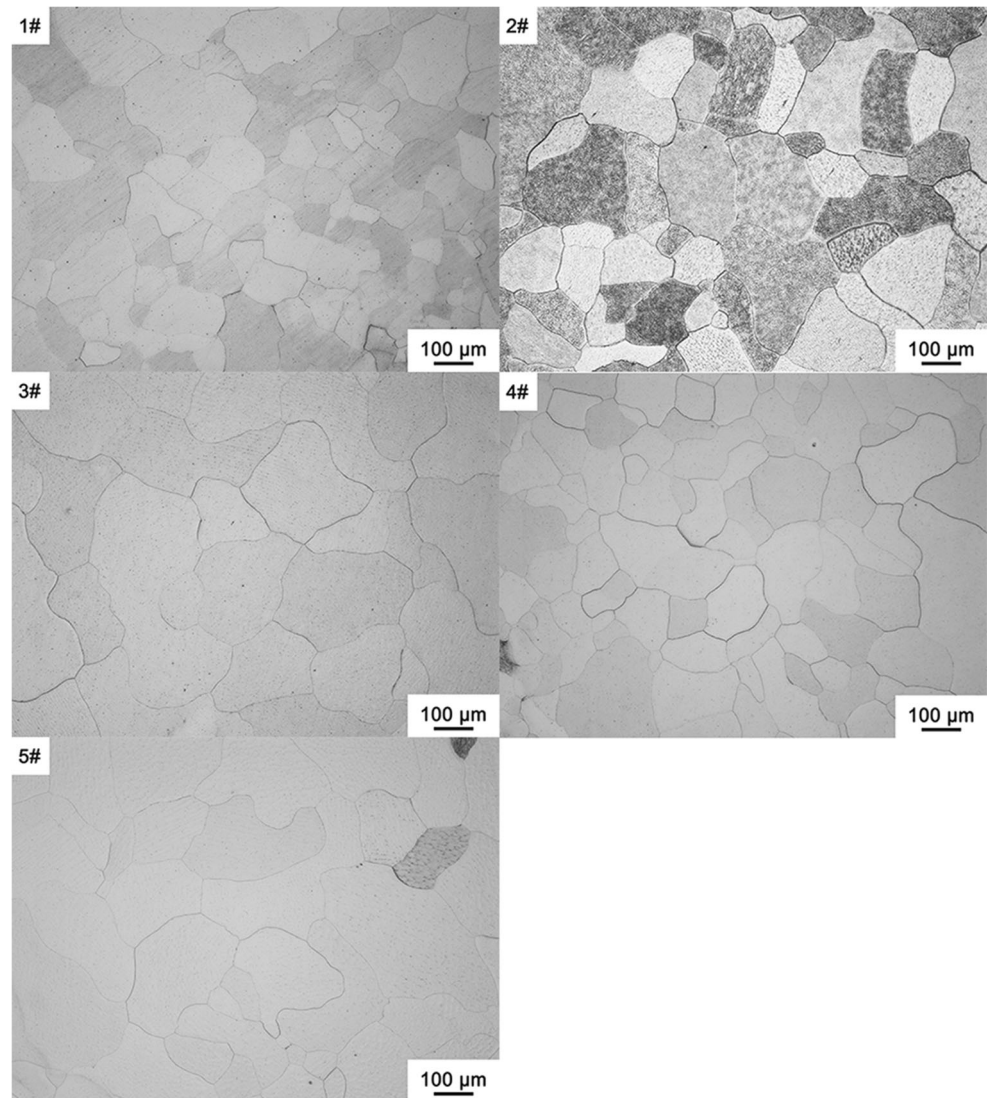
electrode, the counter electrode was a platinum electrode, and the reference electrode was MSE electrode, respectively. The corrosion tests were performed between 0.8 V and 1.6 V at a sweep rate of 1 mV s^{-1} for 50 cycles, which were an approximate simulated battery rapid charge and discharge process. The microstructure and composition of the alloys' corrosion layer on the surface were observed by scanning electron microscopy (SEM; HITACHI-SU3500). After the corrosion, corrosion layer on the surface of the alloys was removed by acetic acid and sodium acetate solution, and the surface of the alloys was observed with a metallographic microscope. Potassium acetate and nitric acid solution were used to convert all the lead compounds in the dissolved layer into Pb^{2+}, and then Pb^{2+} content was determined by chemical titration method to calculate the corrosion rate of different alloys. The corrosion products were removed, and the surface morphology of the alloy was analyzed by metallographic microscope.

Results and discussion

Metallographic microstructure and hardness analysis

The size and uniformity of the grains can affect the corrosion resistance of the alloy, so the metallographic test can be used to observe and analyze the performance of the alloy grains. The mechanical strength of the alloy can be

Table 2 Hardness results of the five alloys

Numbers	Additives	Hardness (HV)
1#	–	20.538
2#	Bi	16.592
3#	Ba	17.520
4#	Sr	23.012
5#	Ge	22.008

Fig. 2 Anodic polarization of alloy electrodes in 1.28 g cm^{-3} H$_2$SO$_4$ from 0.6 to 1.8 V. **a** Anodic polarization curves. **b** The logi-E curves. 1#: Pb-Ca-Sn-Al; 2#: Pb-Ca-Sn-Al-Bi; 3#: Pb-Ca-Sn-Al-Ba; 4#: Pb-Ca-Sn-Al-Sr; 5#: Pb-Ca-Sn-Al-Ge
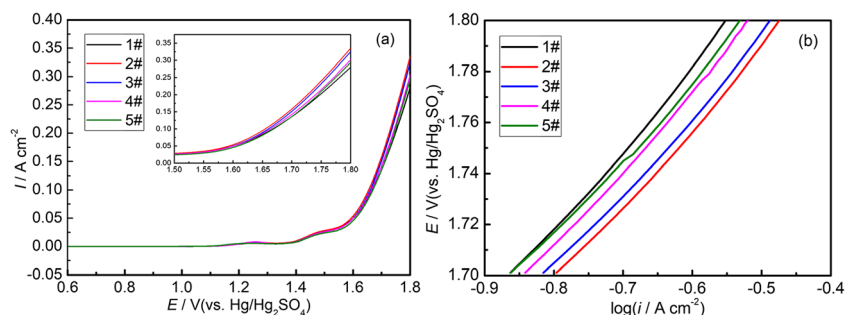
used to pre-determine the deformation and corrosion rate of the grid, and the hardness of the alloy is proportional to the mechanical strength, so the mechanical strength of the alloy can be measured by hardness testing.

The metallographic structures of the different alloys were observed by a metallographic microscope and are shown in Fig. 1. It can be observed that the grain distribution of 1# alloy (Pb-Ca-Sn-Al) is not uniform, which can be ascribed to that Ca is precipitated unevenly from the unit cell and forms intermetallic compounds such as Pb$_3$Ca and Sn$_3$Ca at the grain boundaries. These dispersed precipitated particles are unevenly distributed, hindering the further growth of grains and leading to inhomogeneous grain distribution and the larger diameter gap [16].

Due to the segregation of calcium in the lead-calcium-tin-aluminum alloy, there is large difference between the grain surface and the interior in terms of the chemical composition. Intergranular corrosion is more severe in the lead-calcium-tin-aluminum alloy. The grain size distribution of 2#, 3#, 4#, and 5# samples is similar with 1# alloy (1#: Pb-Ca-Sn-Al, 2#: Pb-Ca-Sn-Al-Bi, 3#: Pb-Ca-Sn-Al-Ba, 4#: Pb-Ca-Sn-Al-Sr, 5#: Pb-Ca-Sn-Al-Ge). However, the grain boundaries of the four group five element modified alloys are more distinct. The grain size of 2#, 3#, and 5# alloys is increased, which may reduce the intergranular corrosion of the alloy theoretically.

The hardness results of the electrodes after polishing are shown in the Table 2. The Vivtorinox hardness comparison of the alloy samples is as follows: 2# < 3# < 1# < 5# < 4#. Compared with the pristine lead-calcium-tin-aluminum quaternary alloys, the hardness decreases with the addition of bismuth and barium; in contrast, the hardness increases with the addition of strontium and germanium. The decrease of the hardness of 2# and 3# alloys may be related to the increased grain size of the alloy.

Maintenance-free performance

Oxygen evolution

At the end of charge or overcharge of the lead-acid battery, PbSO$_4$ is almost completely converted to PbO$_2$ at the positive electrodes. At this time, the side reaction of oxygen evolution is dominant. It was reported that the positive electrode starts to precipitate oxygen when the charge capacity of the positive electrode reaches about 70% [17]. Although oxygen evolving from the positive electrode can be recombined on the lead negative electrode in VRLA, premature evolution of oxygen causes a charging efficiency loss and an increased internal temperature of the battery. Therefore, it is very important to suppress the oxygen evolution.

In order to understand the anodic behavior of oxygen evolution of the alloys, the electrodes were tested by anodic polarization from 0.6 to 1.8 V. The five kinds of alloys exhibit different selectivity of oxygen evolution. Figure 2 a shows the anodic polarization curve of the alloy in 1.28 g cm^{-3} H$_2$SO$_4$ solution, and the polarization curve of 1.5–1.8 V is partially amplified in the figure. Figure 2 b shows the Tafel plots, which is plotted with potential interval data from 1.7 to 1.8 V with a good linear relationship. By linearly fitting the Tafel plots and analyzing the Tafel equation: $E = a + b \times \log |i|$, the relevant kinetic parameters can be obtained. The kinetic parameters of the oxygen evolution reaction are listed in Table 3. The constant a is the oxygen evolution overpotential at a current density of 1 A cm^{-2}, which represents the difficult degree of the oxygen evolution reaction; and the constant b is the slope of the Tafel curve, which represents the relationship between the oxygen evolution reaction rate and the potential. R is the
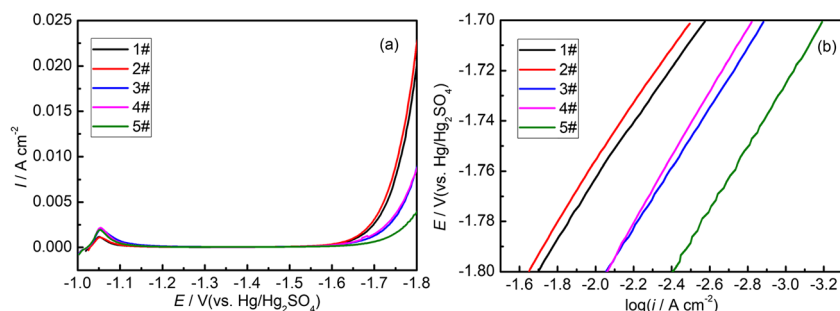
Table 3 Kinetic parameters of the oxygen evolution reaction on Pb alloy electrodes with different additives obtained by LSV method

Numbers	a^a	b^b	R
1#	1.97251	0.31855	0.99659
2#	1.94255	0.30778	0.99629
3#	1.9438	0.30225	0.99607
4#	1.95702	0.30777	0.99752
5#	1.95401	0.29723	0.99582

[a] The oxygen evolution overpotential at a current density of 1 A cm^{-2}
[b] The slope of the Tafel curve

Fig. 3 Cathode polarization of alloy electrodes in 1.28 g cm^{-3} H$_2$SO$_4$ from − 1.0 to − 1.8 V. **a** Cathode polarization curves. **b** The logi-E curves. 1#: Pb-Ca-Sn-Al; 2#: Pb-Ca-Sn-Al-Bi; 3#: Pb-Ca-Sn-Al-Ba; 4#: Pb-Ca-Sn-Al-Sr; 5#: Pb-Ca-Sn-Al-Ge

correlation coefficient of the formula. It can be seen that all the kinetic parameters a decrease with the addition of additives, indicating that the additives decrease the oxygen evolution overpotential of the alloy and promote the oxygen evolution reaction, while the oxygen evolution overpotential of the alloys decreases by up to about 30 mV with Bi or Ba addition [18].

Hydrogen evolution

Generally, the hydrogen evolution of the negative electrode is also an important reason for the water loss in the lead-acid battery. That is why the lead-antimony alloys are not used for long-life maintenance-free batteries because of its low hydrogen evolution overpotential. Therefore, we have studied the cathodic hydrogen evolution behavior of the alloys. Figure 3 a shows the cathodic polarization curve of the alloys in 1.28 g cm^{-3} H$_2$SO$_4$ solution; Fig. 3 b shows the Tafel plots, which is plotted with potential interval data from − 1.7 to − 1.8 V with a good linear relationship. By linearly fitting the Tafel plots and analyzing the Tafel formula: $E = a + b \times \log |i|$, the relevant kinetic parameters can be obtained. The kinetic parameters of the hydrogen evolution reaction are listed in Table 4. The constant a is the hydrogen evolution overpotential at a current density of 1 A cm^{-2}, which represents the difficult degree of the hydrogen evolution reaction. And the constant b is the slope of the Tafel curve, which represents the relationship between the hydrogen evolution reaction rate and the potential. R is the correlation coefficient of the formula. By comparing the value of a, it is shown that Bi has little effect on the hydrogen evolution of the alloy, but Ba, Sr, and Ge effectively suppress the hydrogen evolution of the alloy. Among that, Ge alloy exhibits the most obvious effect on increasing the hydrogen overpotential of the alloy with about 100 mV.

Electrochemical reversibility

Figure 4 shows the cyclic voltammograms of 1# alloy electrode performed between 0.6 V and 1.6 V at the 10th, 20th, 30th, 40th, and 50th cycles in 1.28 g cm^{-3} H$_2$SO$_4$ solution. In the positive sweep, three anodic peaks (a, b, and c) can be

observed at 0.94 V, 1.4 V, and 1.6 V, which are corresponded to the oxidation of Pb to PbO$_x$ ($1 < x < 2$) oxides, formation of β-PbO$_2$ from PbSO$_4$, and oxygen evolution reaction, respectively. In the negative sweep, the reduction peak d at about 1.03 V corresponds to the reduction of PbO$_2$ [19].

It can be seen from the cyclic voltammograms that the peaks of oxidation and reduction currents increase with increasing the number of cyclic tests. The increased surface area of the alloy might be a possible reason for the increased current of peak d [20]. Since the oxygen evolution reaction is accompanied by the test, it is difficult to accurately determine the amount of the anodic oxidation charges in the potential interval. The cathode reduction charges of the anodized product during the reverse sweep are reflected by the d peak, so the growth rate of the cathode reduction charges is used to estimate the anodic oxidation charges. Table 5 lists the reduction peak areas (cathode reduction charges, Q_{red}) and cathode reduction charge growth rates of the five alloy electrodes. It is observed that the Q_{red} and the cyclic numbers show a good linear relationship. The results can be concluded that the growth rates of the alloy with the addition of Bi and Ba are lower than Pb-Ca-Sn-Al alloy, and higher with the addition of Sr and Ge. It is shown that the addition of Bi and Ba can effectively inhibit the growth and accumulation of PbO$_2$ in the corrosion layer of Pb-Ca-Sn-Al alloy. The peak potential and peak current data of the 50th cycle for peak b and peak d in the five alloys are shown in Table 6. It can be seen that the oxidation

Table 4 Kinetic parameters of the hydrogen evolution reaction on Pb alloy electrodes with different additives obtained by LSV method

Numbers	a[a]	b[b]	R
1#	− 1.98980	− 0.11298	0.99894
2#	− 1.99040	− 0.11677	0.99851
3#	− 2.04523	− 0.11936	0.99994
4#	− 2.06745	− 0.13037	0.99967
5#	− 2.10118	− 0.12534	0.99969

[a] The hydrogen evolution overpotential at a current density of 1 A cm^{-2}
[b] The slope of the Tafel curve

Fig. 4 The cyclic voltammograms of 1 #, 2#, 3#, 4#, and 5# alloy electrodes from 0.6 to 1.6 V in 1.28 g cm^{-3} H$_2$SO$_4$ for the 10th, 20th, 30th, 40th, and 50th cycles (scan rate = 5 mV s^{-1}). 1#: Pb-Ca-Sn-Al; 2#: Pb-Ca-Sn-Al-Bi; 3#: Pb-Ca-Sn-Al-Ba; 4#: Pb-Ca-Sn-Al-Sr; 5#: Pb-Ca-Sn-Al-Ge
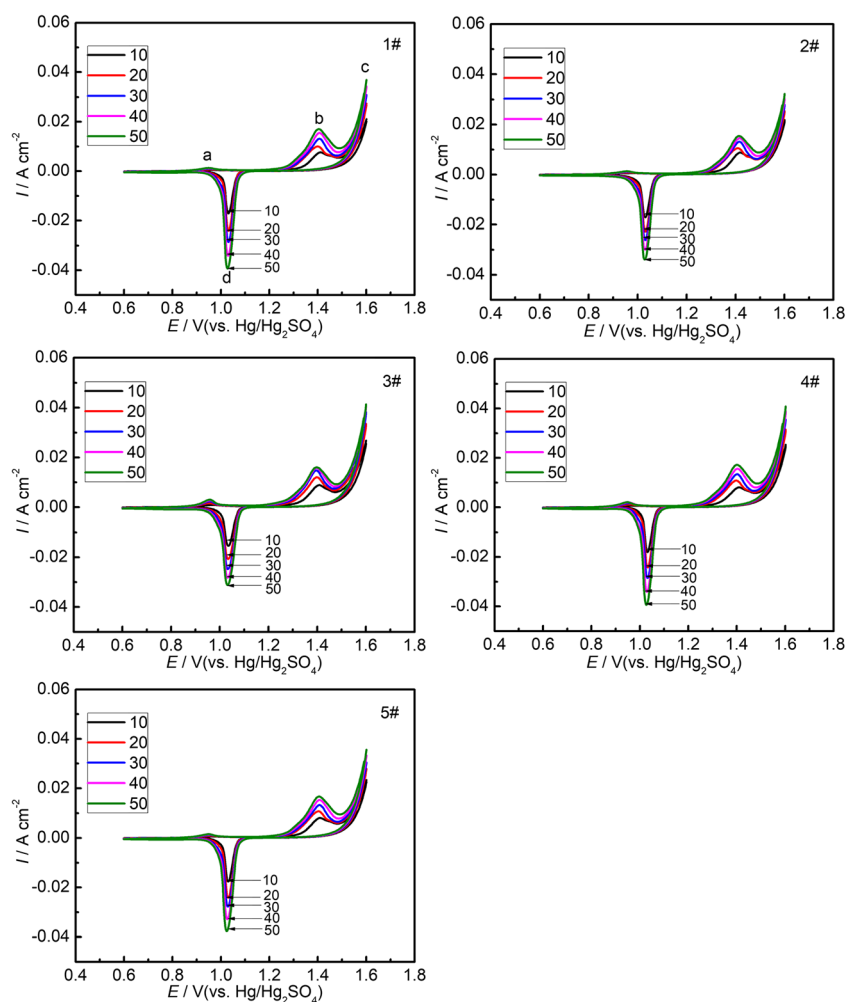
peak current and the reduction peak current of 2# and 3# alloys decrease compared with those of 1# alloy. It is may be related with that the additives of Bi and Ba change the microstructure of the alloy and reduce the accumulation of corrosion products, thus inhibiting the corrosion of Pb-Ca-Sn-Al alloy.

Table 5 Cathodic reduction charges (Q_{red}) of the peak d in the cyclic voltammograms for different alloy electrodes

Cycles/N	Q_{red} (C cm^{-2})				
	1#	2#	3#	4#	5#
10	0.146	0.162	0.154	0.150	0.152
20	0.218	0.228	0.242	0.228	0.234
30	0.280	0.276	0.314	0.294	0.294
40	0.358	0.333	0.378	0.378	0.370
50	0.435	0.391	0.431	0.459	0.446
Growth rate (C cm^{-2} N)	0.0072	0.0056	0.0069	0.0077	0.0072
R^2	0.998	0.998	0.991	0.998	0.998

Study of PbO growth

The anodic oxide layer is mainly composed of Pb (II) in the anodic oxidation potential between − 0.40 V and 0.95 V in the H$_2$SO$_4$ solution [21]. Due to the high resistivity of PbO (about 10^{11} Ω cm [22]), high impedance of anode Pb (II) layer greatly affects the deep cycle performance of the battery. It has been demonstrated that 0.9 V is close to deep discharge potential of the anode [23]. Therefore, the electrodes were selected for 1-h polarization at 0.9 V in 1.28 g cm^{-3} H$_2$SO$_4$ solution.

Table 6 The peak potential and peak current data for peak b and peak d of different alloys for the 50th cycles

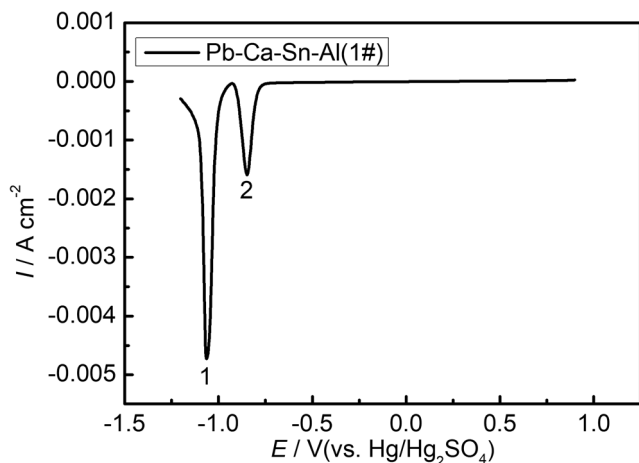| Numbers	E_b (V)	I_b (mA cm^{-2})	E_d (V)	I_d (mA cm^{-2})
1#	1.4008	0.01702	1.0272	−0.03932
2#	1.4102	0.01533	1.0294	−0.03388
3#	1.3934	0.01597	1.0321	−0.03117
4#	1.3971	0.01714	1.026	−0.0394
5#	1.4011	0.0167	1.0251	−0.03768

Fig. 5 Voltammograms of anodic films formed on Pb alloy electrode at 0.9 V for 1 h before sweeping the potential from 0.9 to − 1.2 V in 1.28 g cm^{-3} H$_2$SO$_4$ (scan rate = 2 mV s^{-1})
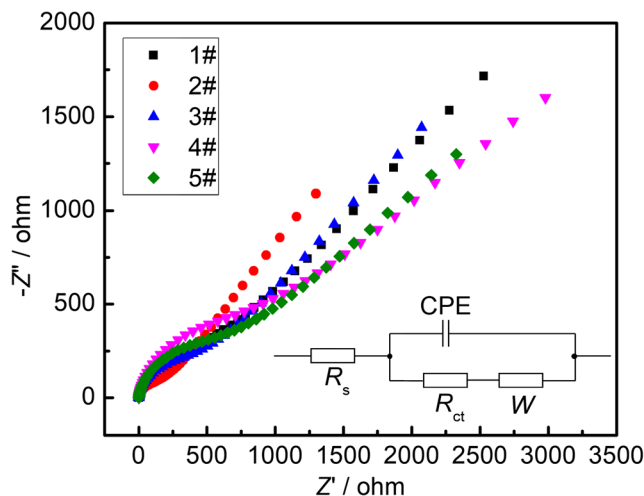

Fig. 6 Nyquist plots of the impedance data and electrical equivalent circuit for different electrodes at 0.9 V in 1.28 g cm^{-3} H$_2$SO$_4$, following polarization at 0.9 V for 1 h. 1#: Pb-Ca-Sn-Al; 2#: Pb-Ca-Sn-Al-Bi; 3#: Pb-Ca-Sn-Al-Ba; 4#: Pb-Ca-Sn-Al-Sr; 5#: Pb-Ca-Sn-Al-Ge

The different alloy electrodes were polarized at 0.9 V for 1 h, then swept to − 1.2 V at a scanning rate of 2 mV s^{-1}. Figure 5 shows the typical voltammograms of anodic films on Pb-Ca-Sn-Al alloy electrode. The voltammograms of other electrodes have similar shapes to Fig. 5, so they are not listed. In Fig. 5, two peaks can be observed, in which peak 1 corresponds to the reduction reaction of PbSO$_4$ to Pb and peak 2 corresponds to the reduction of Pb (II) oxides to Pb [20]. Table 7 lists the comparison of peak potentials and currents of peak 1 and peak 2. It can be seen that the potential of the peak 2 (the reduction of Pb (II) oxides to Pb) of the alloys with the additives of Bi and Ba is more positive than that of Pb-Ca-Sn-Al alloy, and the peak current is much lower. Therefore, it indicates that the electrochemical reduction of Pb (II) on the alloy surface is smaller. The possible explanation is that there are smaller amounts of Pb (II) or higher conductivity corrosion products on the surface of the alloy electrodes [24]. The additions of Bi and Ba can reduce the overpotential potential of anodic Pb (II) oxide film and improve the conductivity of the corrosion layer.

In order to further study the mechanism of different alloy electrodes, the alloy electrode was polarized at 0.9 V for 1 h and then subjected to AC impedance test. Figure 6 shows the Nyquist plots of the different electrodes at open circuit

potential and equivalent circuit diagram. As demonstrated that the high-frequency region is controlled by charge transfer process and the low-frequency region is controlled by ion diffusion process, the electrical equivalent circuit is used to fit the impedance data of different electrodes [25]. R_s, R_{ct}, CPE, and W represent the solution resistance, charge transfer resistance (i.e., the resistance of the Pb (II) film), constant phase element, and Warburg impedance, respectively. Correspondingly, the calculated parameters in the fitting circuit are shown in Table 8. Compared with 1# alloy, the R_{ct} of the alloys with additive Bi and Ba decreases, indicating that less high-impedance Pb (II) oxide is formed on the alloy electrodes [26]. Thus, the addition of Bi and Ba can improve the conductivity of the alloy corrosion layer, probably preventing premature loss of capacity.

Corrosion and morphology evolution

Corrosion test was performed by cyclic voltammetry in a three-electrode system in the electrolyte of 1.28 g cm^{-3} H$_2$SO$_4$ at 50 °C to simulate the actual operating conditions

Table 7 Comparison of peak potentials and currents of the voltammograms in Fig. 7

Numbers	E_1 (V)	$I_{p,1}$ (mA cm^{-2})	E_2 (V)	$I_{p,2}$ (mA cm^{-2})
1#	−1.063	−4.73	−0.848	−1.60
2#	−1.073	−3.95	−0.845	−1.43
3#	−1.08	−4.01	−0.833	−1.51
4#	−1.058	−4.93	−0.87	−1.62
5#	−1.051	−4.28	−0.914	−1.80

Table 8 Resistance of anodic films formed on Pb alloy electrodes with different additives at 0.9 V

Numbers	R_s (Ω cm^{-2})	R_{ct} (Ω cm^{-2})	CPE-T (*10^{-6} F cm^{-2})	CPE-P	W (*10^3 Ω cm^{-2})
1#	0.445	201.7	5.727	0.93340	6.15
2#	0.472	94.45	10.934	0.91234	3.34
3#	0.504	186.6	8.643	0.91673	5.24
4#	0.493	222.4	7.176	0.92421	5.32
5#	1.206	341.3	16.419	0.84408	4.06

Fig. 7 SEM photographs of the surface of the corrosion layers after 50 cycles of cycle voltammetry at 1 mV s^{-1} from 0.8 to 1.6 V in 1.28 g cm^{-3} H$_2$SO$_4$ at 50 °C (at ×5000 and ×500). 1#: Pb-Ca-Sn-Al; 2#: Pb-Ca-Sn-Al-Bi; 3#: Pb-Ca-Sn-Al-Ba; 4#: Pb-Ca-Sn-Al-Sr; 5#: Pb-Ca-Sn-Al-Ge

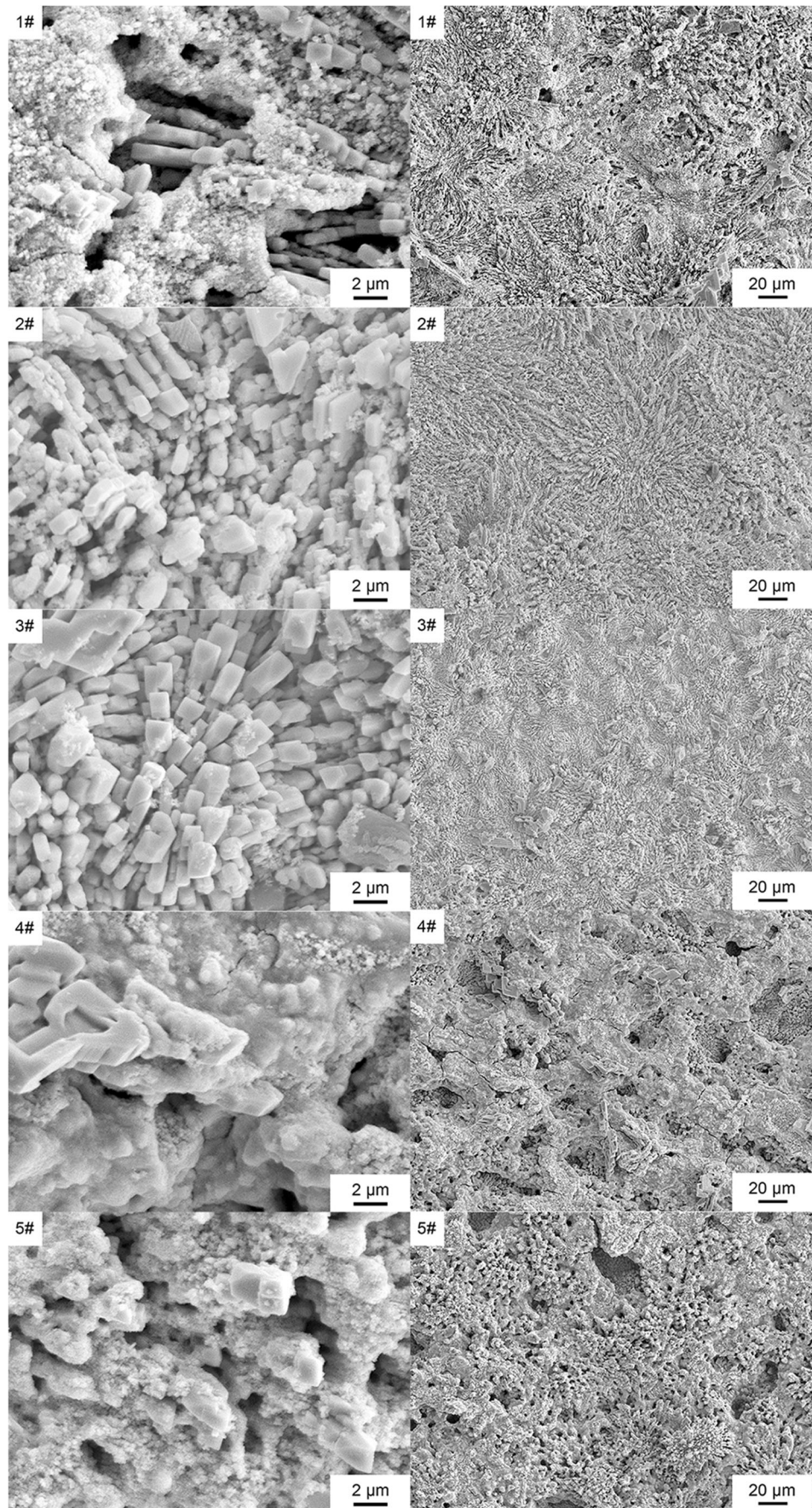**Table 9** Constant current corrosion rate of alloys

| Numbers	Additives	Corrosion rate ($mg\ h^{-1}\ cm^{-2}$)
1#	–	0.517
2#	Bi	0.439
3#	Ba	0.467
4#	Sr	0.537
5#	Ge	0.564

of the positive grid. Figure 7 shows the scanning electron microscope (SEM) photographs of the surface corrosion layers after 50 cycles for the five samples at ×5000 and ×500. The compositions of the corrosion layer were analyzed by an energy dispersive spectrometer (EDS). The SEM and the EDS analyses of the corrosion layer reveal that the corrosion products are almost PbO_2 and $PbSO_4$. PbO_2 was irregular

paste-like crystal structure, and $PbSO_4$ was regular small crystal particle structure [27].

In Fig. 7, it could be seen that the surface corrosion layer of 1# alloy was mainly composed of PbO_2. In addition, the structure of the corrosion layer was loose and even cracked, exhibiting a perforated structure which appeared in the corrosion layer. The structures of 4# and 5# corrosion layers are similar to those of 1#, and there are more perforation holes in the corrosion layer. However, the corrosion products of 2# and 3# alloys on the corrosion layer show more obvious aggregated and dense state. Many lead sulfates have not been further oxidized to lead dioxide on the surface of 2# and 3# alloys. The uniform and dense corrosion layer could reduce the contact area between the alloy matrix and sulfuric acid and inhibit further corrosion of the alloy matrix. Therefore, 2# and 3# alloys will have better corrosion resistance.

Table 9 illustrates the corrosion rate of the alloys under the cyclic voltammetry test, where the corrosion rates of 2# and

Fig. 8 The metallographic microstructure of the alloys after removing the corrosion layer, following 50 cycles of cycle voltammetry at $1\ mV\ s^{-1}$ from 0.8 to 1.6 V in $1.28\ g\ cm^{-3}$ H_2SO_4 at 50 °C. 1#: Pb-Ca-Sn-Al; 2#: Pb-Ca-Sn-Al-Bi; 3#: Pb-Ca-Sn-Al-Ba; 4#: Pb-Ca-Sn-Al-Sr; 5#: Pb-Ca-Sn-Al-Ge
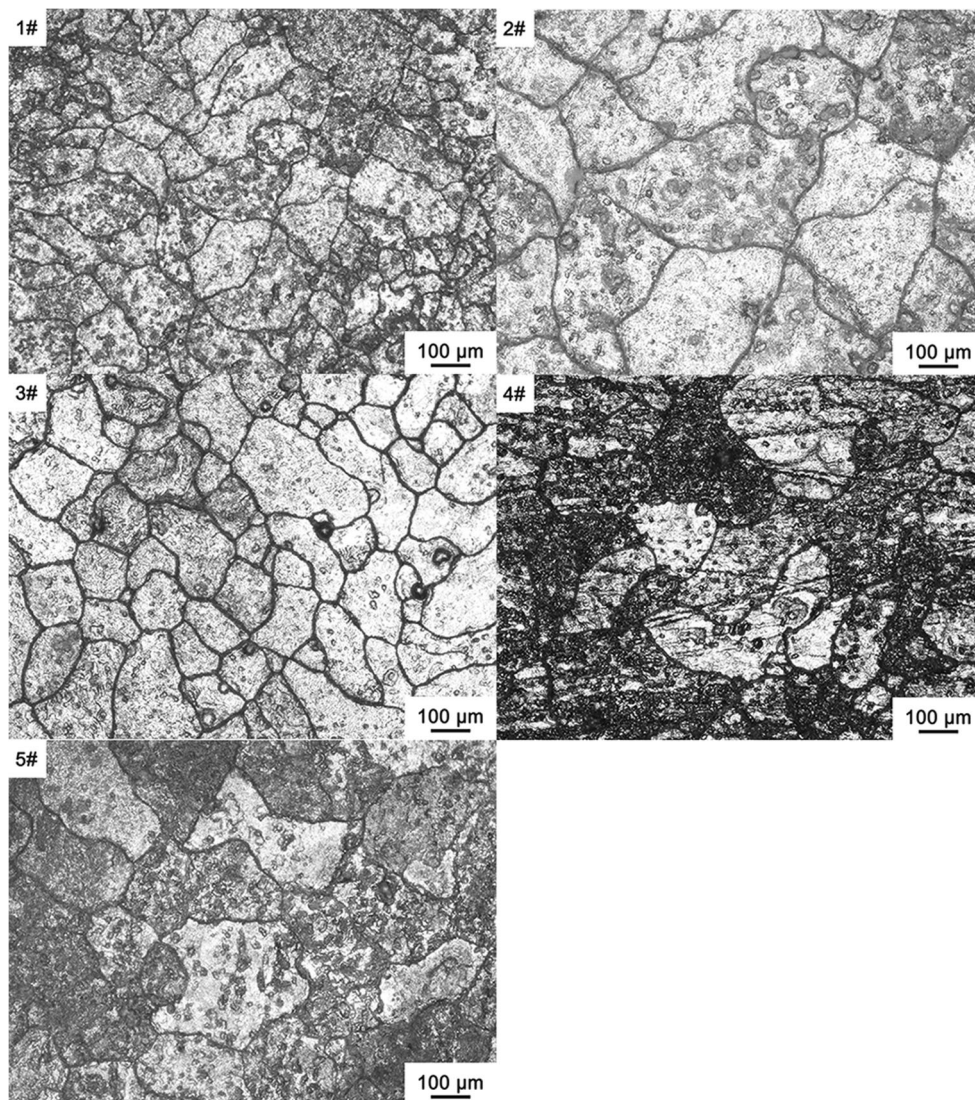
3# alloy samples were decreased, and the corrosion rates of 4# and 5# alloy samples were increased as compared with 1# alloy sample. The results indicate that the corrosion resistance of lead-calcium-tin-aluminum alloys was improved with the addition of Bi and Ba in this test.

Figure 8 presents the metallographic microstructure of all the alloys after removing the surface corrosion layer by acetic acid and sodium acetate solution. By comparing the metallographic microstructure of the corrosion-removed layer, it is known that different alloy electrodes exhibit different corrosion behaviors. The electrodes of 1#, 4#, and 5# alloys appeared serious grain corrosion and grain boundary corrosion. The grains of 2# and 3# alloys are much intact, and the grain boundaries are clear. The alloy corrosion of 2# and 3# samples occurs mainly in the grain boundary, where the grains are completed with less point corrosion. Therefore, it can be deduced that 2# and 3# alloys (with the additives of Bi and Ba in Pb-Ca-Sn-Al alloy) can reduce the segregation of the alloy components in the grain and form a relatively stable metallography, improving the corrosion resistance of the alloy.

Conclusion

In summary, we synthesized five kinds of lead-calcium-tin-aluminum alloys using four additives. We evaluated the effect of the fifth additive element on the physical and electrochemical properties of the alloys. We found that the additives of Bi and Ba can increase the grain size of the alloy and reduce the intergranular corrosion of Pb-Ca-Sn-Al alloy. However, the hardness of the alloys will slightly decrease.

Bi, Ba, Sr, and Ge all cause a slight decrease in the anodic overpotential of the alloy, but cause the hydrogen evolution overpotential to rise to varying degrees. The results of LSV, CV, and EIS show that the growth of Pb (II) and PbO_2 in corrosion layer on Pb-Ca-Sn-Al alloy can be inhibited by adding Bi or Ba, and the corrosion resistance of the alloy can be improved. Adding Bi or Ba to the alloy inhibits the grain corrosion of the alloy. The surface of the corrosion layer is regular and dense, which protects the alloy matrix. The corrosion rate of the alloy decreases significantly. Bi and Ba are excellent alloy additives and can be added to positive grid alloys for long-life lead-acid batteries.

References

1. Lannelongue J, Cugnet M, Guillet N, Kirchev A (2017) Electrochemistry of thin-plate lead-carbon batteries employing alternative current collectors. J Power Sources 352:194–207

2. Tong PY, Zhao RR, Zhang RB, Yi FY, Shi G, Li AJ, Chen HY (2015) Characterization of lead (II)-containing activated carbon and its excellent performance of extending lead-acid battery cycle life for high-rate partial-state-of-charge operation. J Power Sources 286:91–102

3. Wang LY, Zhang H, Zhang WF, Cao GP, Zhao HL, Yang YS (2017) Enhancing cycle performance of lead-carbon battery anodes by lead-doped porous carbon composite and graphite additives. Mater Lett 206:113–116

4. Monahov B, Pavlov D (1994) Influence of antimony on the structure and the degree of hydration of the anodic PbO_2 layer formed on Pb-Sb electrodes. J Electrochem Soc 141(9):2316–2326

5. Li DG, Zhou GS, Zhang J, Zheng MS (2007) Investigation on characteristics of anodic film formed on PbCaSnCe alloy in sulfuric acid solution. Electrochim Acta 52(5):2146–2152

6. Prengaman RD (2001) Challenges from corrosion-resistant grid alloys in lead acid battery manufacturing. J Power Sources 95(1-2):224–233

7. Rocca E, Steinmetz J, Weber S (1999) Mechanism of formation of dense anodic films of PbO on lead and lead alloys in sulfuric acid: use of an 18 O tracer. J Electrochem Soc 146(1):54–58

8. Caillerie JL, Albert L (1997) Lead-calcium alloy development: quality improvement. J Power Sources 67(1-2):279–281

9. Lam LT, Haigh NP, Rand DAJ, Manders JE (2000) Further demonstration of improved performance from lead-acid batteries manufactured with bismuth-bearing high-purity lead. J Power Sources 88(1):2–10

10. Lam LT, Haigh NP, Rand DAJ (2000) Understanding the mechanism by which bismuth improves lead-acid battery capacity. J Power Sources 88(1):11–17

11. Li AJ, Cheni Y, Chen HY, Shu D, Li WS, Wang H, Dou CL, Zhang W, Chen S (2009) Electrochemical behavior and application of lead-lanthanum alloys for positive grids of lead-acid batteries. J Power Sources 189(2):1204–1211

12. Furukawa J, Nehyo Y, Shiga S (2004) Development of new positive-grid alloy and its application to long-life batteries for automotive industry. J Power Sources 133(1):25–31

13. Lam LT, Douglas JD, Pillig R, Rand DAJ (1994) Minor elements in lead materials used for lead/acid batteries 1. Hydrogen- and oxygen-gassing characteristics. J Power Sources 48(1-2):219–232

14. Chen HY, Li S, Li AJ, Shu D, Li WS, Dou CL, Wang Q, Xiao GM, Peng SG, Chen S, Zhang W, Wang H (2007) Lead-samarium alloys for positive grids of valve-regulated lead-acid batteries. J Power Sources 168(1):79–89

15. Li DG, Wang JD, Chen DR (2012) Influence of ytterbium on the electrochemical property of PbCaSn alloy in sulfuric acid solution. J Power Sources 210:163–171

16. Lakshmi CS, Manders JE, Rice DM (1998) Structure and properties of lead-calcium-tin alloys for battery grids. J Power Sources 73(1): 23–29

17. Bose CSC, Hampson NA (1987) A review of oxygen recombination in the sealed lead-acid cell. J Power Sources 19(4):261–267

18. Tang LP, Li AJ, Chen HY, Li H, Chen Q, Zhou HW, Wei WW, Zhang W, Hu J, Dou CL, Wang H, Finlow D (2011) The electrochemical performances of a novel lead-sodium binary grid alloy for lead-acid batteries. Electrochim Acta 56(12):4566–4570

19. Liu HT, Zhang XH, Zhou YB, Yang CX, Zhou WF (2003) The anodic films on lead alloys containing rare-earth elements as positive grids in lead acid battery. Mater Lett 57(29):4597–4600

20. Zhou WF, Cheng XL (1985) The anodic film of lead-antimony alloys in sulfuric acid solution-I. The kinetics of the early stage anodic film growth. Acta Chim Sin 43:333–339

21. Pavlov D, Poulieff CN, Klaja E, Iordanov N (1969) Dependence of the composition of the anodic layer on the oxidation potential of lead in sulfuric acid. J Electrochem Soc 116(3):316–319

22. Liu HT, Yang J, Liang HH, Zhuang JH, Zhou WF (2001) Effect of cerium on the anodic corrosion of Pb-Ca-Sn alloy in sulfuric acid solution. J Power Sources 93(1-2):230–233

23. Shervedani RK, Isfahani AZ, Khodavisy R, Hatefi-Mehrjardi A (2007) Electrochemical investigation of the anodic corrosion of Pb-Ca-Sn-Li grid alloy in H_2SO_4 solution. J Power Sources 164(2):890–895

24. Pour-Ali S, Aghili MM, Davoodi A (2015) Electrochemical corrosion behavior of Pb-Ca-Sn-Sm grid alloy in H_2SO_4 solution. J Alloys Compd 652:172–178

25. Li H, Guo WX, Chen HY, Finlow DE, Zhou HW, Dou CL, Xiao GM, Peng SG, Wei WW, Wang H (2009) Study on the microstructure and electrochemical properties of lead-calcium-tin-aluminum alloys. J Power Sources 191(1):111–118

26. Guo WX, Shu D, Chen HY, Li AJ, Wang H, Xiao GM, Dou CL, Peng SG, Wei WW, Zhang W, Zhou HW, Chen S (2009) Study on the structure and property of lead tellurium alloy as the positive grid of lead-acid batteries. J Alloys Compd 475(1-2):102–109

27. Wu YM, Zhao RR, Zhou HW, Zhang DJ, Zhao W, Chen HY (2016) Synthesis and application of a novel Cu/RGO@Pb alloy for lead-acid batteries. Electrochim Acta 222:116–122